Korea-Australia Rheology Journal
Vol. 18, No. 2, June 2006 pp. 51-65

A mathematical model of blood flow and convective diffusion processes in constricted bifurcated arteries

S. Chakravarty* and S. Sen
Department of Mathematics, Visva-Bharati University, Santiniketan 731 235, India.
(Received January 19, 2006; final revision received April 20, 2006)

Abstract

Of concern in the present theoretical investigation is the study of blood flow and convection-dominated diffusion processes in a model bifurcated artery under stenotic conditions. The geometry of the bifurcated arterial segment having constrictions in both the parent and its daughter arterial lumen frequently appearing in the diseased arteries causing malfunction of the cardiovascular system, is constructed mathematically with the introduction of suitable curvatures at the lateral junction and the flow divider. The streaming blood contained in the bifurcated artery is treated to be Newtonian. The flow dynamical analysis applies the two-dimensional unsteady incompressible nonlinear Navier-Stokes equations for Newtonian fluid while the mass transport phenomenon is governed by the convection diffusion equation. The motion of the arterial wall and its effect on local fluid mechanics is, however, not ruled out from the present model. The main objective of this study is to demonstrate the effects of constricted flow characteristics and the wall motion on the wall shear stress, the concentration profile and on the mass transfer. The ultimate numerical solutions of the coupled flow and diffusion processes following a radial coordinate transformation are based on an appropriate finite difference technique which attain appreciable stability in both the flow phenomena and the convection-dominated diffusion processes.

1. Introduction

Hemodynamics has long been suspected of being involved in many arterial diseases and, of course, good correlation has been observed between the localization of the lesions and the flow disturbances around bends and curvatures in larger arteries. The transport phenomena of blood always play a key role to the understanding of arterial diseases, in general, and the transport of macromolecules with dissolved gases to and through the arterial wall influences more on the growth and the development of atherogenetic processes, in particular. In order to gain more information about the fluid dynamic factor in atherogenesis, quite a good number of experimental and theoretical studies have been carried out in the recent past and special attention has always been centered on the flow analysis in arterial bifurcations. A comprehensive review concerning the hemodynamical studies of arterial bifurcations has been successfully conducted by Lou and Yang (1992). One of the proposed several hypotheses for the role of hemodynamics in the genesis of atherosclerosis is that the occurrence of atherosclerosis is closely related to high shear stress. Fry (1968) pointed out that a moderately elevated wall shear stress or pressure can increase the permeability of endothelial cells. Reidy and Bowyer (1997) reported from their experiments on rabbits that focal endothelial damage was consistently found on and distal to aortic flow dividers. The experimental findings of Liepsch and Moravec (1984) and Liepsch (1990) indicated that in regions with high shear stress the blood shells are damaged or their surface is deformed and then the corpuscles stick to the wall followed by a deposition in low shear stress region. For the sake of a complete understanding of the flow phenomena through arterial bifurcation from the physiological point of view with respect to atherosclerotic lesions, one must have the knowledge of atherosclerosis, knowledge of hemodynamics and the correlations between them. Moreover, under in vivo situations, the transportation of blood in the circulatory system depends on the pumping action of the heart producing a pulsatile pressure gradient throughout the arterial network.

The numerical methods are often found to be quite useful in supporting experimental methods which have got their own importance especially for the determination of the flow variables like wall shear stresses which can be quite difficult to obtain in experiments. Quite a few numerical studies concentrate on transport processes in the micro-

*Corresponding author: santabrata2004@yahoo.co.in

circulation (Singh *et al.*, 1982; McIntire *et al.*, 1989; Bassingthwaitghte *et al.*, 1992) but major attention has yet been focused on the transport phenomena in large arteries through numerical investigations. There could have been many reasons behind not carrying out such studies. One possible cause may be due to the fact that most of these transport phenomena are highly convection dominated owing to the low diffusion coefficient of the principal constituents governing transportation of blood.

Friedman and Ehrlich (1975) made an introductory attempt to investigate the convective effect of steady blood flow on diffusion process in an arterial system. They modelled the flow in a simplified two-dimensional arterial bifurcation and obtained an analytical boundary layer solution for the concentration at the vessel wall and hence they avoided to carry out any numerical investigation of the transport equation. Subsequently Back *et al.* (1977) investigated pulsatile oxygen transport to multiple non-constricted plaque regions numerically by finite difference technique and observed a strong reduction in oxygen transport on the back side of plaques at incipient flow separation zones. Another numerical simulation of mass transfer in a sudden expansion tube model under pulsatile condition was framed by Ma *et al.* (1994) where the effect of separated flow on luminal mass transport and on the wall mass transfer coefficient was recorded. It has been an well established fact that in the arterial system the fluid dynamic factors affect blood phase transport and vascular wall properties to a considerable extent. Hence for a complete understanding of the transport phenomena one needs to incorporate the potentiality of treating simultaneously the luminal transport in the blood phase and shear dependent variations in intimal permeability. Having such considerations in mind, Rappitsch and Perktold (1996) studied numerically the steady convective diffusion processes in axisymmetric tube in the presence of a local constriction by applying a passive transport law for the flux at the wall and physiologically realistic values for the flow of mass transfer parameters. They treated their investigation with two different models for the solute wall flux – one assuming constant wall permeability and the other considering shear-dependent wall permeability.

Keeping in view of the motivation as mentioned above a careful attempt is made to formulate an unsteady two - dimensional bifurcation model of arteries theoretically in the present investigation in order to estimate some of the important characteristics of transport phenomena governing pulsatile blood flow in aortic bifurcation. The time-dependent geometry of the bifurcated artery developed by Chakravarty and Mondal (1997) has been updated further in the light of requirement for the present simulation. The present symmetrical aorta is assumed to have a couple of stenoses - one in the parent arterial lumen and the other in the daughter one. The Y-shaped bifurcation is regarded as symmetrical about the axis of the trunk with an angle of 90° bifurcation and the inclusion of the necessary curvature at the lateral junctions and the flow divider certainly improves resemblance to the in vivo situation in a sense that when the blood vessel bifurcates, it does it gradually. The geometry under consideration hence bears the potential to rule out the possibility of any discontinuity and large flow separation zones or non-existent flow separation zones. The flowing blood contained in the bifurcated artery is treated as Newtonian. The cylindrical coordinate system has been taken for analytical formulation. Due attention has also been paid to the effect of arterial wall motion on local fluid mechanics but not on the stresses and strains in the vascular wall. The nonlinear equations of motion governing blood flow and the convection-diffusion equation governing mass transport following the radial coordinate transformation are solved numerically by a suitable finite difference technique with the appropriate use of boundary and matching conditions in concert with the physical representations of the problem. For the diffusive flux at the wall in the transport phenomena, the wall permeability is treated to be shear-dependent which is believed to be an important feature for a physiologically realistic simulation of mass transfer process as evidenced from the experimental observations (Jo *et al.*, 1991; Tarbell, 1993). An extensive quantitative analysis has finally been performed at the end of the paper through graphical representations of the results together with their discussions at length so as to validate the applicability of the present simulation.

2. Formulation of the problem

In order to formulate the mathematical model under consideration, the following assumptions are taken into account:

- The arteries forming bifurcations are symmetrical about the trunk axis and circular cylinders of finite length having the angle of 90° between two branches.
- Both the parent aorta and its daughter artery possess a mild stenosis each in their lumen.
- The flow is considered two dimensional unsteady so that both the radial and axial velocity components come into play.
- The mass transport is coupled to the velocity field of the blood stream.
- Blood is treated to be a homogeneous Newtonian fluid of constant density.
- The arterial wall motion is introduced into the local fluid mechanics but not on the stresses and the strains on the vascular wall.
- The appropriate curvatures are introduced at the lateral junctions and the flow divider of the bifurcated arteries successfully so that one can rule out all possibilities of any discontinuity causing large flow separation zones or non-existent flow separation zones.

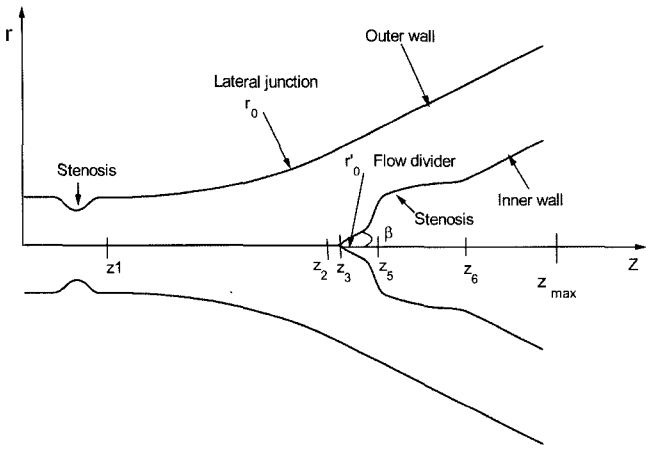

Fig. 1. Schematic diagram of the constricted bifurcated arterial segment.

- The wall permeability is treated to be shear-dependent in context with mass transfer.

Let (r, θ, z) be the coordinates of the representative material point in the cylindrical polar coordinate system where the z-axis is taken along the axis of the trunk while (r, θ) are taken along the radial and the circumferential directions respectively. The geometry of the bifurcated artery (cf. Fig. 1) having two symmetrical mild stenoses one in the parent aorta and the other in its branch is constructed mathematically of which the outer wall geometry is described by

$$R_1(z,t) =$$

$$\begin{cases} a.a_1(t), & 0\le z\le d', d'+l_0\le z\le z_1, \\ \left[a-\dfrac{4\tau_m}{l_0^2}-\{l_0(z-d')-(z-d')^2\}\right]a_1(t), & d'\le z\le d'+l_0, \\ [a+r_0-\sqrt{r_0^2-(z-z_1)^2}]a_1(t), & z_1\le z\le z_2, \\ [2r_1\sec\beta+(z-z_2)\tan\beta]a_1(t), & z_2\le z\le z_{max}, \end{cases} \tag{1}$$

while that for the inner wall is given by

$$R_2(z,t) =$$

$$\begin{cases} 0, & 0\le z\le z_3, \\ \sqrt{r'^2_0-(z-z_3-r'_0)^2}\,b_1(t), & z_3\le z\le z_3+r'_0(1-\sin\beta), \\ (z-z_2)\tan\beta\, b_1(t), & z_3+r'_0(1-\sin\beta)\le z\le z_5, z_6\le z\le z_{max}, \\ \sqrt{r'^2_2-(z_6-z)^2}\,b_1(t), & z_5\le z\le z_6, \end{cases} \tag{2}$$

where $R_1(z, t)$ and $R_2(z, t)$ are the respective radii of the outer and inner wall, a the unconstricted radius of the parent artery, r_1 the radius of the daughter artery, (r_0, r'_0) the respective radii of curvatures for the lateral junctions and the flow divider, l_0 the length of the stenosis at a distance d' from the origin, z_1 the location of the onset of the lateral junction, z_2 the offset of the lateral junction, z_3 the apex, (z_5, z_6) the respective locations corresponding to the onset and offset of the stenosis in the daughter artery, β be the semi-bifurcation angle and τ_m represents the height of the stenosis. Here z_{max} denotes the finite length of the bifurcated artery under study.

The various parameters involved in the above expressions (1) and (2) may be defined as

$$a_1(t) = 1-(\cos\omega t-1)k\exp(-k\omega t),$$

$$b_1(t) = \frac{1}{a_1(t)},$$

$$z_2 = z_1+(a-2r_1\sec\beta)\frac{\sin\beta}{\cos\beta-1},$$

$$r_0=\frac{a-2r_1\sec\beta}{\cos\beta-1},\quad r'_0=\frac{(z_3-z_2)\sin\beta}{1-\sin\beta},\quad r'_2=(z_6-z_2)\tan\beta \tag{3}$$

and $z_3 = z_2 + q$, where q is chosen to be a small number lying in the range $0.1\le q\le 0.5$ for compatibility of the geometry and k is a constant.

Let us consider the flow of blood to be unsteady, nonlinear, axisymmetric, two dimensional and fully developed where blood is treated to be an incompressible Newtoninan fluid. The Navier-Stokes' equations and the equation of continuity that govern the motion of blood may be written in the cylindrical co-ordinate system as

$$\rho\left(\frac{\partial u}{\partial t}+u\frac{\partial u}{\partial r}+w\frac{\partial u}{\partial z}\right)=-\frac{\partial p}{\partial r}+\mu\left(\frac{\partial^2 u}{\partial r^2}+\frac{1}{r}\frac{\partial u}{\partial r}-\frac{u}{r^2}+\frac{\partial^2 u}{\partial z^2}\right), \tag{4}$$

$$\rho\left(\frac{\partial w}{\partial t}+u\frac{\partial w}{\partial r}+w\frac{\partial w}{\partial z}\right)=-\frac{\partial p}{\partial r}+\mu\left(\frac{\partial^2 w}{\partial r^2}+\frac{1}{r}\frac{\partial w}{\partial r}+\frac{\partial^2 w}{\partial z^2}\right) \tag{5}$$

and $$\frac{\partial u}{\partial r}+\frac{u}{r}+\frac{\partial w}{\partial z}=0, \tag{6}$$

where $u\equiv u(r,z,t)$ and $w\equiv w(r,z,t)$ are the radial and the axial velocity components of the streaming blood respectively, p the pressure, ρ the density and μ represents the viscosity of blood. The convection-diffusion equation describing the mass transport which is coupled to the velocity field of the blood stream is given by

$$\frac{\partial c}{\partial t}+u\frac{\partial c}{\partial r}+w\frac{\partial c}{\partial z}=D\left(\frac{\partial^2 c}{\partial z^2}+\frac{\partial^2 c}{\partial r^2}+\frac{1}{r}\frac{\partial c}{\partial r}\right), \tag{7}$$

where c represents the solute or gas-concentration and D is the constant coefficient of diffusion. Moreover, the pumping action of the heart is represented by the pressure gradient $\frac{\partial p}{\partial z}$ appearing in (5) produced by it, the form of which has been taken from Burton (1996) as

$$-\frac{\partial p}{\partial z}=A_0+A_1\cos\omega t,\quad t>0 \tag{8}$$

where A_0 is the constant amplitude of the pressure gradient, A_1 is the amplitude of the pulsatile component giving rise to systolic and diastolic pressure. Here $\omega = 2\pi f_p$, f_p being the pulse frequency.

3. Boundary conditions

As no radial flow takes place along the axis of the parent aorta and there is no shear rate of the fluid along the axis of the trunk, one may write as

$$u(r,z,t)=0,\ \frac{\partial w(r,z,t)}{\partial r}=0 \ \text{ on } r=0 \text{ for } 0\le z\le z_3. \quad (9)$$

The velocity boundary conditions on the outer wall surface are taken as

$$u(r,z,t)=\alpha\frac{\partial R_1}{\partial t},\ w(r,z,t)=0 \ \text{ on } r=R_1(z,t) \text{ for all } z, \quad (10)$$

while those on the inner half (daughter) are assumed to be

$$u(r,z,t)=\alpha\frac{\partial R_2}{\partial t},\ w(r,z,t)=0 \ \text{ on } r=R_2(z,t) \text{ for } z\ge z_3 \quad (11)$$

in which $\alpha=1$ for $z<z_3$ and $\alpha=\sec\beta$ for $z\ge z_3$.

The concentration gradient at the axis may be taken to be the symmetry condition given by

$$\frac{\partial c(r,z,t)}{\partial r}=0 \ \text{ on } r=0 \text{ for } 0\le z\le z_3. \quad (12)$$

At the inlet, the concentration is assumed to be constant while the concentration gradient at the apex may be assumed to be equal to be zero, that is

$$c(r,z,t)=c_0 \text{ at } z=0 \text{ and } \frac{\partial c(r,z,t)}{\partial z}=0 \text{ at } z=z_3. \quad (13)$$

Moreover, it is assumed that there is no velocity field of the flowing blood in the presence of constant initial concentration of oxygen when the entire system is at rest, that means, initially

$$u(r,z,t)=0,\ w(r,z,t)=0 \text{ and } c(r,z,t)=c_0 \text{ at } t=0 \quad (14)$$

4. Method of solution

Generally in a problem dealing with the coupling of the fluid mechanics with the vessel wall mechanics, $R_1(z,t)$ and $R_2(z,t)$ would not be prescribed, but instead, could be computed as a part of the solution of the coupled problem. Here both $R_1(z,t)$ and $R_2(z,t)$ are specified and hence we focus our attention on hemodynamic factors only.

Introducing a radial coordinate transformation, given by

$$\xi=\frac{r-R_2}{R_1-R_2}=\frac{r-R_2}{R}, \quad (15)$$

which possesses the effect of immobilizing the bifurcated vessel wall in the transformed coordinate ξ. Here $R(z,t)=R_1(z,t)-R_2(z,t)$.

Using the transformation, the equations (5)-(7) take the following form

$$\frac{\partial w}{\partial t}=-\frac{1}{\rho}\frac{\partial p}{\partial z}+\frac{1}{R}\frac{\partial w}{\partial \xi}\left[\left(\xi\frac{\partial R}{\partial t}+\frac{\partial R_2}{\partial t}\right)+\frac{\mu}{\rho(\xi R+R_2)}\right.$$
$$\left.-\frac{\mu}{\rho}\left\{\frac{\partial^2 R_2}{\partial z^2}+\xi\frac{\partial^2 R}{\partial z^2}-\frac{2}{R}\frac{\partial R}{\partial z}\left(\xi\frac{\partial R}{\partial z}+\frac{\partial R_2}{\partial z}\right)\right\}\right]$$
$$+\frac{\mu}{\rho R^2}\left[1+\left(\xi\frac{\partial R}{\partial z}+\frac{\partial R_2}{\partial z}\right)^2\right]\frac{\partial^2 w}{\partial \xi^2}-\frac{u}{R}\frac{\partial w}{\partial \xi}$$
$$-w\left[\frac{\partial w}{\partial z}-\frac{1}{R}\left(\xi\frac{\partial R}{\partial z}+\frac{\partial R_2}{\partial z}\right)\frac{\partial w}{\partial \xi}\right]+\frac{\mu}{\rho}\frac{\partial^2 w}{\partial z^2}, \quad (16)$$

$$\frac{1}{R}\frac{\partial u}{\partial \xi}+\frac{u}{\xi R+R_2}+\frac{\partial w}{\partial z}-\frac{1}{R}\frac{\partial w}{\partial \xi}\left(\xi\frac{\partial R}{\partial z}+\frac{\partial R_2}{\partial z}\right)=0, \quad (17)$$

$$\frac{\partial c}{\partial t}=\frac{1}{R}\frac{\partial c}{\partial \xi}\left[\left(\xi\frac{\partial R}{\partial t}+\frac{\partial R_2}{\partial t}\right)+\left(w+\frac{D}{R}\frac{\partial R}{\partial z}\right)\left(\xi\frac{\partial R}{\partial z}+\frac{\partial R_2}{\partial z}\right)-u\right.$$
$$\left.-D\left(\xi\frac{\partial^2 R}{\partial z^2}+\frac{\partial^2 R_2}{\partial z^2}\right)+\frac{D}{\xi R+R_2}\right]+w\frac{\partial c}{\partial z}+\frac{D}{R^2}\left[\left(\xi\frac{\partial R}{\partial z}+\frac{\partial R_2}{\partial z}\right)^2+1\right]$$
$$\times\frac{\partial^2 c}{\partial \xi^2}+D\frac{\partial^2 c}{\partial z^2}. \quad (18)$$

Based upon the consideration of negligible variation of pressure within the arterial cross section, that is $p=p(z,t)$ as the radius of the artery is much smaller than its length, one may disregard the radial Navier-Stokes equation (4). Although the effect of arterial stenosis and branching on the motion of blood is important because of convective acceleration, its effect on the radial motion of the artery is negligible. Because of the small radial velocity and acceleration, the radial variation of pressure within the artery can also be neglected. This assumption is well established and authenticated by several researchers (Womersley, 1957; Ling and Atabek, 1972; Imaeda and Goodman, 1980; Deshpande *et al.*, 1976 and Pedley 1980).

The boundary conditions (9) - (14) are also transformed according to (15)

$$u(\xi,z,t)=0,\ \frac{\partial w(\xi,z,t)}{\partial \xi}=0 \ \text{ on } \xi=0 \text{ for } 0\le z\le z_3, \quad (19)$$

$$u(\xi,z,t)=\alpha\frac{\partial R_1}{\partial t},\ w(\xi,z,t)=0 \ \text{ on } \xi=1 \text{ for all } z, \quad (20)$$

$$u(\xi,z,t)=\alpha\frac{\partial R_2}{\partial t},\ w(\xi,z,t)=0 \ \text{ on } \xi=0 \text{ for } z\ge z_3, \quad (21)$$

$$\frac{\partial c(\xi,z,t)}{\partial \xi}=0 \ \text{ on } \xi=0 \text{ for } 0\le z\le z_3, \quad (22)$$

$$c(\xi, z, t) = c_0 \text{ at } z = 0, \quad \frac{\partial c(\xi,z,t)}{\partial z} = 0 \text{ at } z = z_3 \tag{23}$$

$$\text{and } u(\xi, z, 0) = 0, \quad w(\xi, z, 0) = 0, \quad c(\xi, z, 0) = c_0. \tag{24}$$

Multiplying both the sides of (17) by $(\xi R + R_2)$ and integrating with respect to ξ, one obtains

$$u(\xi,z,t) = \left(\xi\frac{\partial R}{\partial z} + \frac{\partial R_2}{\partial z}\right)w(\xi,z,t) + \frac{R_2}{\xi R + R_2}u(0,z,t) - \frac{R}{\xi R + R_2}\int_0^{\xi}(\xi R + R_2)\frac{\partial w}{\partial z}d\xi - \frac{1}{\xi R + R_2}\int_0^{\xi}\left(2\xi R\frac{\partial R}{\partial z} + R_2\frac{\partial R}{\partial z} + R\frac{\partial R_2}{\partial z}\right)w d\xi. \tag{25}$$

Using the boundary condition (20), the equation (25) may take the following form

$$-\int_0^1(\xi R + R_2)\frac{\partial w}{\partial z}d\xi = \int_0^1\left[\left(2\xi\frac{\partial R}{\partial z} + \frac{R_2}{R}\frac{\partial R}{\partial z} + \frac{\partial R_2}{\partial z}\right)w + \frac{R_1}{R}\left\{\alpha\frac{\partial R_1}{\partial t} - \frac{R_2}{R_1}u(0,z,t)\right\}f(\xi)\right]d\xi$$

in which $f(\xi)$ is an arbitrary function satisfying $\int_0^1 f(\xi)d\xi = 1$.

The approximation has been used consisting of the equality between the integrals to integrands. In other words, we suppose that the arbitrary function $f(\xi)$ exists so that

$$(\xi R + R_2)\frac{\partial w}{\partial z} + \left(2\xi\frac{\partial R}{\partial z} + \frac{R_2}{R}\frac{\partial R}{\partial z} + \frac{\partial R_2}{\partial z}\right)w + \frac{R_1}{R}\left\{\alpha\frac{\partial R_1}{\partial z} - \frac{R_2}{R_1}u(0,z,t)\right\} \times f(\xi) = 0.$$

The function $f(\xi)$ must also satisfy the condition $f(1) = 0$ because it has to be $\left.\frac{\partial w}{\partial z}\right|_{\xi=1} = 0$. Without any loss of generality one can assume $f(\xi) = -4\xi(\xi^2 - 1)$ which satisfies all the necessary conditions mentioned above.

Thus the above relation becomes

$$u(\xi,z,t) = \left(\xi\frac{\partial R}{\partial z} + \frac{\partial R_2}{\partial t}\right)w + \frac{R_2}{\xi R + R_2}u(0,z,t) + \frac{R_1\xi^2}{\xi R + R_2}\left\{\alpha\frac{\partial R_1}{\partial t} + \frac{R_2}{R_1}u(0,z,t)\right\}(2 - \xi^2). \tag{26}$$

Introducing (26) into (16) one obtains

$$\frac{\partial w}{\partial t} = -\frac{1}{\rho}\frac{\partial p}{\partial z} + \frac{1}{R}\frac{\partial w}{\partial \xi}\left[\left(\xi\frac{\partial R}{\partial t} + \frac{\partial R_2}{\partial t}\right) + \frac{\mu}{\rho(\xi R + R_2)}\left\{\frac{\partial^2 R_2}{\partial z^2} + \xi\frac{\partial^2 R}{\partial z^2} - \frac{2}{R}\frac{\partial R}{\partial z}\left(\xi\frac{\partial R}{\partial z} + \frac{\partial R_2}{\partial z}\right)\right\} - \frac{R_2}{\xi R + R_2}u(0,z,t) - \frac{R_1\xi^2}{\xi R + R_2}\left\{\alpha\frac{\partial R_1}{\partial t} - \frac{R_2}{R_1}u(0,z,t)\right\}(2 - \xi^2)\right] + \frac{\mu}{\rho R^2}\left[1 + \left(\xi\frac{\partial R}{\partial z} + \frac{\partial R_2}{\partial z}\right)^2\right]\frac{\partial^2 w}{\partial \xi^2} + \frac{\mu}{\rho}\frac{\partial^2 w}{\partial z^2} - w\frac{\partial w}{\partial \xi}. \tag{27}$$

The velocity components of the blood stream are determined from (27) and (26) numerically subject to the stated boundary conditions as an initial step. Subsequently, the coupled transport equation (18) is also solved numerically with the knowledge of the quantitative results of the velocity components of the fluid.

5. Finite difference approximation

The finite difference scheme for solving the equations (27), (26) and (18) is based on the forward difference representation for the time derivative and the central difference formula for all the spatial derivatives in the following manner:

$$\frac{\partial w}{\partial t} = \frac{w_{i,j}^{k+1} - w_{i,j}^k}{\Delta t}, \quad \frac{\partial w}{\partial \xi} = \frac{w_{i,j+1}^k - w_{i,j-1}^k}{2\Delta\xi}, \quad \frac{\partial w}{\partial z} = \frac{w_{i+1,j}^k - w_{i-1,j}^k}{2\Delta z},$$

$$\frac{\partial^2 w}{\partial z^2} = \frac{w_{i+1,j}^k - 2w_{i,j}^k - w_{i-1,j}^k}{(\Delta z)^2}, \quad \frac{\partial^2 w}{\partial \xi^2} = \frac{w_{i,j+1}^k - 2w_{i,j}^k - w_{i,j-1}^k}{(\Delta\xi)^2},$$

$$\frac{\partial c}{\partial t} = \frac{c_{i,j}^{k+1} - c_{i,j}^k}{\Delta t}, \quad \frac{\partial c}{\partial \xi} = \frac{c_{i,j+1}^k - c_{i,j-1}^k}{2\Delta\xi}, \quad \frac{\partial c}{\partial z} = \frac{c_{i+1,j}^k - c_{i-1,j}^k}{2\Delta z},$$

$$\frac{\partial^2 c}{\partial z^2} = \frac{c_{i+1,j}^k - 2c_{i,j}^k - c_{i-1,j}^k}{(\Delta z)^2}, \quad \frac{\partial^2 c}{\partial \xi^2} = \frac{c_{i,j+1}^k - 2c_{i,j}^k - c_{i,j-1}^k}{(\Delta\xi)^2},$$

With the introduction of these finite difference approximations of the time and the spatial derivatives in (27) and (18), one can easily transform them into the following difference equations:

$$w_{i,j}^{k+1} = w_{i,j}^k + \Delta t\left[-\frac{1}{\rho}\left(\frac{\partial p}{\partial z}\right)_i^k + (A_{i,j}^k + B_{i,j}^k + C_{i,j}^k + D_{i,j}^k)\left(\frac{w_{i,j+1}^k - w_{i,j-1}^k}{2\Delta\xi R_i^k}\right) + F_{i,j}^k(w_{i,j+1}^k - 2w_{i,j}^k + w_{i,j-1}^k) + G(w_{i+1,j}^k - 2w_{i,j}^k + w_{i-1,j}^k) + Hw_{i,j}^k(w_{i+1,j}^k - w_{i-1,j}^k)\right], \tag{28}$$

$$c_{i,j}^{k+1} = c_{i,j}^k + \Delta t(d_{ij}^k c_{i,j+1}^k + e_{ij}^k c_{i,j-1}^k + f_{ij}^k c_{i+1,j}^k + g_{ij}^k c_{i-1,j}^k + l_{ij}^k c_{i,j}^k), \tag{29}$$

where the respective coefficients $A_{i,j}^k$, $B_{i,j}^k$, $C_{i,j}^k$ etc. involving (28) and d_{ij}^k, e_{ij}^k, f_{ij}^k etc. of (29) have got their expressions included in Appendix. The discretisation has been performed by defining $z_i = (i-1)\Delta z$, $i = 1(1)M+1$ and $\xi_j = (j-1)\Delta\xi$, $j = 1(1)N+1$ for the entire bifurcated arterial segment under consideration in which Δz and $\Delta\xi$ are the respective increments in the axial and the radial directions. Also the boundary conditions (19)-(24) are similarly discretized following the finite difference approximation as

$$u^k_{i,1}=0,\quad w^k_{i,2}=w^k_{i,1}\quad \text{for } z_i\le z_3 \tag{30}$$

$$u^k_{i,N+1}=\alpha\frac{\partial R^k_{1i}}{\partial t},\quad w^k_{i,N+1}=0\quad \text{for all } z_i \tag{31}$$

$$u^k_{i,1}=\alpha\frac{\partial R^k_{2i}}{\partial t},\quad w^k_{i,1}=0\quad \text{for all } z_i\ge z_3 \tag{32}$$

$$c^k_{i,2}=c^k_{i,1}\quad \text{for } z_i\le z_3 \tag{33}$$

$$c^k_{1,j}=c_0,\quad c^k_{M+1,j}=c^k_{M,j}\quad \text{for all } \xi_j \tag{34}$$

$$\text{and } u^1_{i,j}=u_0,\quad w^1_{i,j}=w_0\quad \text{for all } i,j. \tag{35}$$

After having determined the solution of (28) by making use of the relevant boundary conditions numerically for the axial velocity component of the flow, the corresponding velocity in the radial direction can be directly obtained from (26). Subsequently, the concentration profile describing the mass transport can be determined from (29) with the use of the results of the flow-field thus obtained.

The volumetric flow rate or the net flux for both the parent aorta ($z\le z_3$) and the daughter ($z\ge z_3$) arteries can be determined by following the truncated Taylor's series expansions in order to express the velocity components in the daughter arteries along the oblique line inclined at an angle β with the trunk axis, given by

$$u^k_{i,k}{}'=u^k_{i,j}-\frac{\partial u^k_{i,j}}{\partial z}(j-1)\Delta\xi\tan\beta+\frac{1}{2}\frac{\partial^2 u^k_{i,j}}{\partial z^2}[(j-1)\Delta\xi\tan\beta]^2+\cdots\cdots \tag{36}$$

$$w^k_{i,k}{}'=w^k_{i,j}-\frac{\partial w^k_{i,j}}{\partial z}(j-1)\Delta\xi\tan\beta+\frac{1}{2}\frac{\partial^2 w^k_{i,j}}{\partial z^2}[(j-1)\Delta\xi\tan\beta]^2+\cdots\cdots \tag{37}$$

and consequently their discretised versions with first order approximations give

$$u^k_{i,k}{}'=u^k_{i,j}-\left(\frac{j-1}{2\Delta\xi}\right)(u^k_{i+1,j}-u^k_{i-1,j})\tan\beta\Delta\xi+O(h^2), \tag{38}$$

$$w^k_{i,k}{}'=w^k_{i,j}-\left(\frac{j-1}{2\Delta\xi}\right)(w^k_{i+1,j}-w^k_{i-1,j})\tan\beta\Delta\xi+O(h^2), \tag{39}$$

h being the length of the mesh.

Hence the volumetric flow rate (Q_p) for the parent ($z\le z_3$) aorta and the net flux (Q_d) for the daughter ($z\ge z_3$) arteries become

$$Q_p=2\pi R^k_i\left[R^k_i\int_0^1\xi_j w^k_{i,j}d\xi_j+R^k_{2i}\int_0^1 w^k_{i,j}d\xi_j\right], \tag{40}$$

$$\begin{aligned}Q_d=&-\pi R_i^{k^2}\int_0^{\frac{\sec\beta}{2}}\xi_j(w^k_{i,j}{}'\cos\beta+u^k_{i,j}{}'\sin\beta)d\xi_j\\&-\pi R^k_i R^k_{2i}\int_0^{\frac{\sec\beta}{2}}(w^k_{i,j}{}'\cos\beta+u^k_{i,j}{}'\sin\beta)d\xi_j\\&+\pi R_i^{k^2}\int_{\frac{\sec\beta}{2}}^{\sec\beta}\xi_j(w^k_{i,j}{}'\cos\beta+u^k_{i,j}{}'\sin\beta)d\xi_j\\&+\pi R^k_i R^k_{2i}\int_{\frac{\sec\beta}{2}}^{\sec\beta}(w^k_{i,j}{}'\cos\beta+u^k_{i,j}{}'\sin\beta)d\xi_j.\end{aligned} \tag{41}$$

For the diffusive flux along the arterial tube one can also obtain the respective solute flux along the trunk and the daughter ones from the following as

$$q_p=2\pi\int_0^1\xi c(\xi,z,t)d\xi, \tag{42}$$

$$q_d=2\pi\int_0^{\sec\beta}\xi c_r(\xi,z,t)d\xi, \tag{43}$$

$$\text{where } c_r=\left[c(\xi,z,t)-\xi\tan\beta\frac{\partial c}{\partial z}\right]\cos\beta, \tag{44}$$

so that the net diffusive flux along the arterial tube becomes $Q=q_p+q_d$.

For the solute flux (q_w) at the outer and the inner wall (daughter) of the bifurcated arteries, a model is chosen with shear-dependent permeability as

$$q_w=-D\frac{\partial c}{\partial n}\Big|_{wall}=g(|\tau_w|)c_w, \tag{45}$$

where n is the unit normal vector pointing outward, c_w is the wall concentration and $g(|\tau_w|)$ represents the shear-dependent wall permeability function defined by $g(|\tau_w|)=B|\tau_w|$, B being the constant proportionality factor.

Finally, the wall shear stresses on the parent outer wall [$r=R_1(z,t)$] and the daughter inner wall [$r=R_2(z,t)$] are obtained, whose derived expressions should be read as

$$\tau_{out}=\mu\left[\alpha\frac{\partial^2 R_1}{\partial z\partial t}-\frac{1}{R\Delta z}\frac{\partial R_1}{\partial z}\left(\alpha\frac{\partial R_1}{\partial z}-u^k_{i,N}\right)-\frac{1}{R\Delta\xi}w^k_{i,N}\right], \tag{46}$$

$$\tau_{in}=\mu\left[\alpha\frac{\partial^2 R_2}{\partial z\partial t}-\frac{1}{R\Delta z}\frac{\partial R_2}{\partial z}\left(u^k_{i,2}-\alpha\frac{\partial R_2}{\partial z}\right)-\frac{1}{R\Delta z}w^k_{i,2}\right], \tag{47}$$

Here the suffixes "out" and "in" indicate the outer and the inner wall of the bifurcated artery respectively.

6. Numerical results and discussion

With a view to examining the applicability of the present mathematical model, a specific numerical illustration has been undertaken with the use of the existing data for the various physical parameters encountered in the analysis. The numerical computations have been performed with the primary objectives to estimate the unsteady concentration profile at various locations of the bifurcated arterial segment, the mean concentration distribution, the wall shear stresses, the diffusive flux along the arterial duct and the

solute flux at both the outer and the inner wall together with the effects of stenosis and the wall distensibility on them quantitatively. The effect of bifurcation on the concentration profiles is however not ruled out from the present bifurcated flow phenomena. The following data have been made use of in order to carry out the numerical computations (Milnor, 1982; Lou and Yang, 1992; Rappitsch and Perktold, 1996):

$a = 11$ mm, $l_0 = 15$ mm, $d = 5$ mm, $z_{max} = 60$ mm, $\tau_m = 0.3a$, $f_p = 1.2$ Hz, $\beta = 45^\circ$, $\rho = 1.05 \times 10^3$ Kg m^{-3}, $\mu = 0.0035$ N m^{-2} s, $r_1 = 0.7a$, $k = 0.1$, $z_1 = 10$ mm, $z_5 = 40$ mm, $D = 1.6 \times 10^{-4}$ mm s^{-1}, $A_0 = 10$ Kg m^{-2} s^{-2}, $A_1 = 0.2\,A_0$, $B = 9 \times 10^{-6}$ m^3 N^{-1} s^{-1}, $c_0 = 2.58 \times 10^{-6}$ ml mm^{-3}

The explicit iterative finite difference scheme employed in the present analysis for solving (28) as an initial step towards numerical computation has been found to converge satisfactorily with the respective spacings $\Delta z = 1.0$ and $\Delta\xi = 0.01$ along the axial and the radial directions. The necessary convergence of the results quantified has been successfully achieved with the desired precision for a grid size of 60×100 and the results are displayed through the Figs. 2-22 along with their discussions at length in order to substantiate the applicability of the present model.

For the present unsteady simulation, the inlet profiles of the velocity-field are computed and plotted in Figs. 2(a) and (b) for three different time periods. Both these figures also include the corresponding profiles in the absence of stenosis and the wall motion. The axial velocity profiles at the inlet appear to be flattened more than half way towards the wall keeping their respective maxima on the axis and then to diminish gradually towards the wall surface to approach minimum value (zero) on the outer surface. One may observe from the unsteady behaviour of the flow profile that the axial velocity gets enhanced with the advancement of time more towards the axis than in the vicinity of the wall surface. The effect of constriction on the axial velocity profile is found to be quite significant but there is meagre influence of the wall motion on the flow profile. Unlike the behaviour of the axial velocity profile, the radial velocity profiles at the inlet appear to decline from zero on the axis as one moves away from it and eventually to increase towards the wall to attain some finite values on the wall surface. Conversely, the topmost curve (Fig. 2(b)) corresponding to $t = 2$s in the absence of stenosis is noted to increase from zero on the axis, rises to definite peak and then slightly diminishes towards the wall surface. The deviation of the results thus obtained for the curves corresponding to $t = 2$s clearly quantifies the effect of stenosis on the radial velocity profile while the inlet radial velocity assumes uniformly zero value when the wall motion is totally withdrawn from the system under consideration. It is worthwhile to mention that the flatness of the axial velocity profile at the inlet gradually disappears as the flow

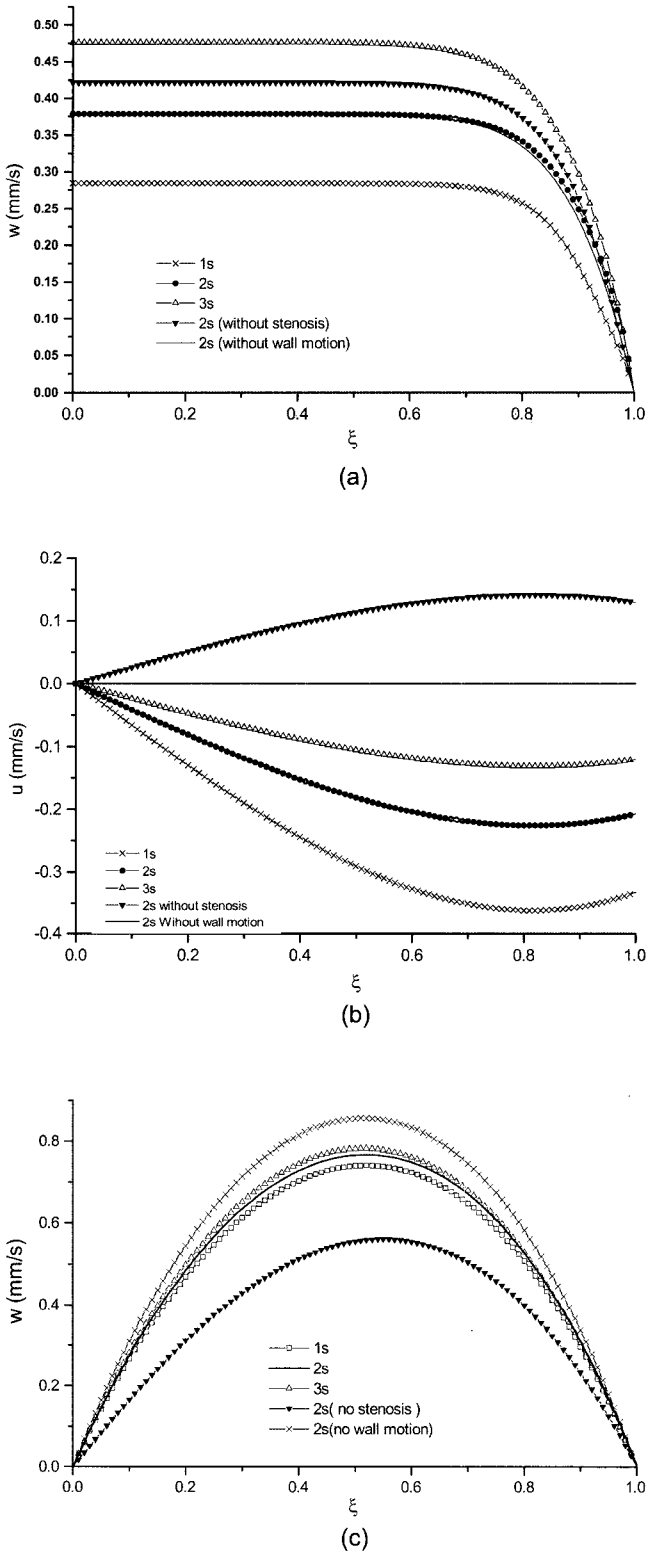

Fig. 2. (a) The axial velocity profile of the streaming blood at the inlet for different time periods, (b) the radial velocity profile of the streaming blood at the inlet for different time periods and (c) axial velocity profile of blood in the daughter artery at a critical location of the stenosis for different time periods.

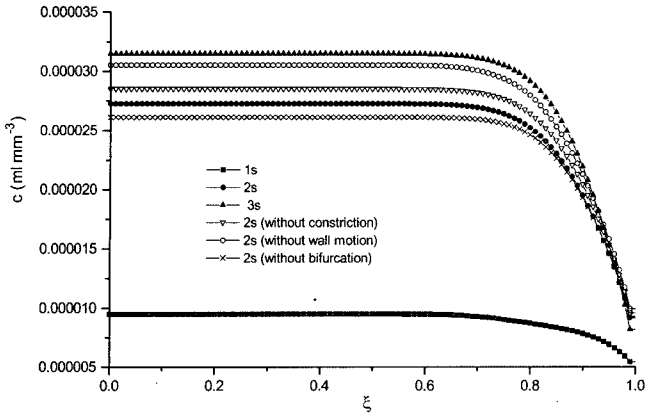

Fig. 3. The concentration profile for the parent aorta at the pre-stenotic region ($z = 4$ mm) for different time periods.

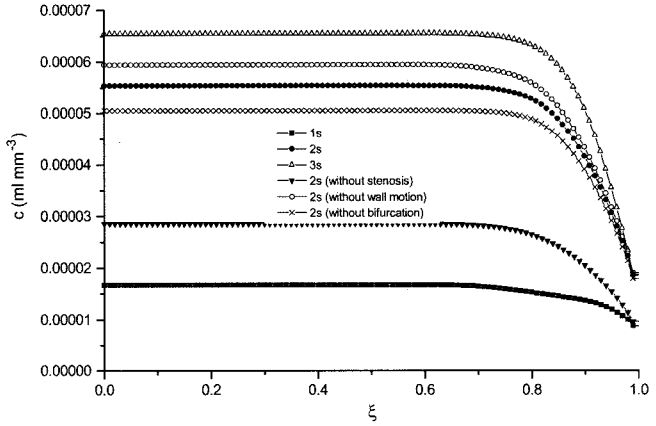

Fig. 4. The concentration profile for the parent aorta at the maximumconstricted site ($z = 6$ mm) for different time periods.

progresses and profile takes parabolic shape the moment the flow becomes fully developed. For the purpose of validating the assumption of the axial symmetry, the Fig. 2(c) represents the behaviour of the axial velocity profile in the daughter artery at a critical location of the stenosis for three different time periods. The influence of vessel wall distensibility and the presence of constriction on the velocity profile can be recorded to be significant from the present figure. All the curves of this figure appear to be symmetrical with respect to mid-position from inner to outer daughter arterial walls. Such observation certainly validates the assumption of axial symmetry that does not breakdown even the recirculation zone is comparable in size.

Fig. 3 illustrates the behaviour of the concentration profiles of the solute in the streaming blood media at a specific location of $z = 4$ mm corresponding to the pre-stenotic region of the parent aorta for three different time periods. It also includes the corresponding results for three more cases: (i) by disregarding the presence of constriction, (ii) by withdrawing wall motion and (iii) by disregarding arterial bifurcation. All the curves appear to be diminishing from their respective maxima at the axis as one moves away from it and finally they approach and converge to a minimum value on the wall surface. The increasing trend of the concentration profile with the advancement of time reflects its behaviour in the unsteady state. If one disregards the presence of constriction in the parent arterial lumen, the concentration of the solute becomes higher as observed from the results of the relevant curves plotted at $t = 2$s. On the other hand, a substantial increase in magnitudes of the concentration profile is noted when the arterial wall motion is totally withdrawn from the system under study. The magnitudes of the concentration, however, get reduced for a straight arterial tube than for a bifurcated one. Thus analyzing the characteristics of all the results of the present figure, one may conclude that the effects of constriction, the wall distensibility and of the arterial bifurcation on the concentration profile are significant and they should be regarded as key factors in such a simulation.

The concentration profiles of the solute at the stenotic region ($z = 6$ mm) of the parent aorta where it assumes the maximum constriction are shown in Fig. 4 for different time periods. Although the results representing the concentration profiles of the solute appear to be analogous in nature to those of Fig. 3 but here the effect of constriction is noted to be quite significant in the sense that the concentration decays sharply in the absence of stenosis unlike the feature of Fig. 3. The concentration grows up faster in the stenotic region as the oxygen gets trapped more in the constricted zone than in the unconstricted one. The results of Fig. 5 corresponding to post-stenotic region ($z = 10$ mm) show meagre effect of constriction on the concentration profile. However, the effects of wall motion and of bifurcation are noted to be similar irrespective of the locations at the onset of the stenosis, at the throat of the stenosis and the offset of the constriction. Analyzing all the results of Figs. 3-5, one can conclude that concentration of the solute increases with the arterial narrowing and with bifurcation but decreases with vessel wall distensibility.

The results of Fig. 6 show the concentration profiles at the apex of the bifurcated artery for different time periods. The present figure also includes the corresponding profiles by disregarding the stenosis, the wall motion and the bifurcation. The shape of the profile changes largely with the advancement of time from 1s to 2s and from 2s to 3s unlike those of Figs. 3-5. However, the effects of stenosis and the wall distensibility on the concentration profile of the solute are quite meager at the apex compared to the other specific sites of the parent aorta. The magnitudes of the present results further indicate that the concentration decays more at the apex than at any other locations of the parent aorta.

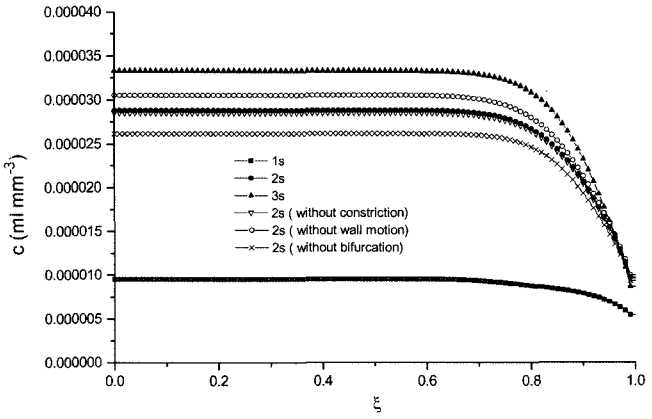

Fig. 5. The concentration profile for the parent aorta at the post-stenotic region ($z = 10$ mm) for different time periods.

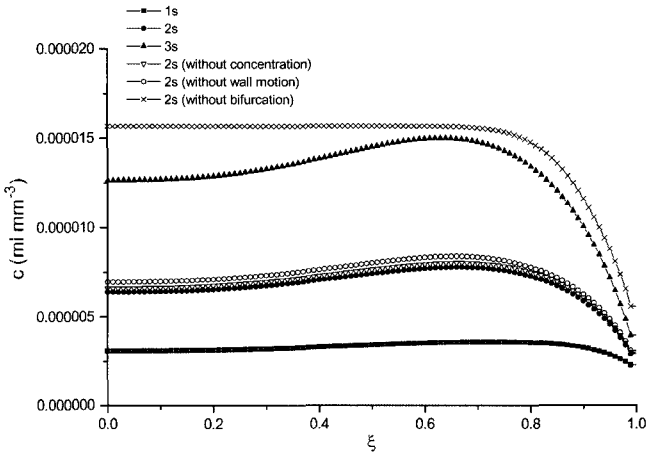

Fig. 6. The concentration profile at the apex ($z = z_3$) of the bifurcated artery for different time periods.

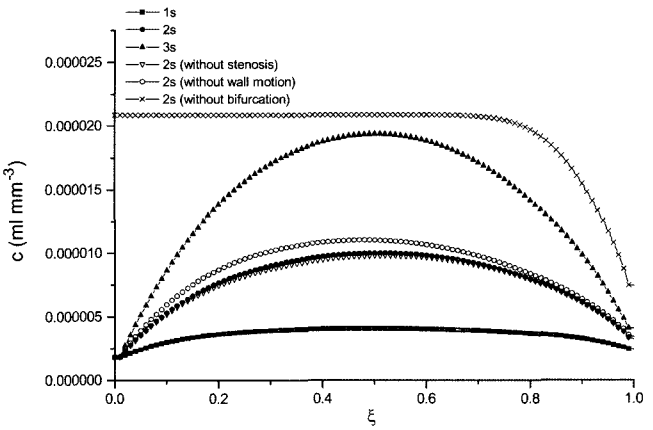

Fig. 7. The concentration profile for the daughter artery at the pre-stenotic region ($z = 40$ mm) for different time periods.

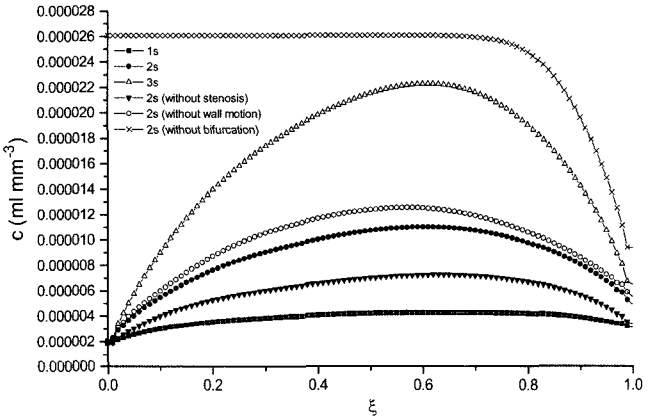

Fig. 8. The concentration profile for the daughter artery at the throat of thestenosis ($z = 45$ mm) for different time periods.

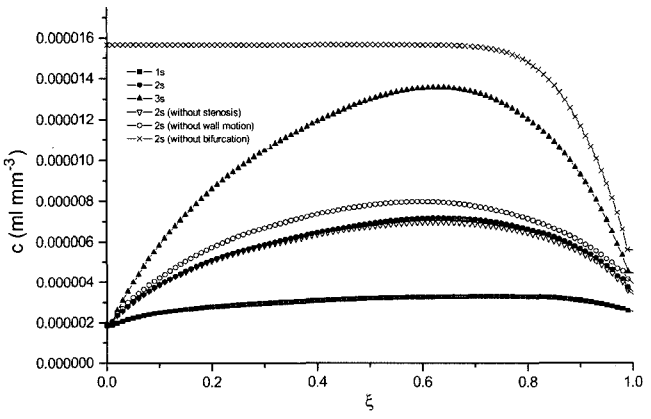

Fig. 9. The concentration profile for the daughter artery at the post-stenotic region ($z = 51$ mm) for different time periods.

The results of the Figs. 7-9 exhibit the concentration profiles of the daughter artery in the unsteady state at three different locations of $z = 40$ mm, 45 mm and 51 mm corresponding to pre-stenotic, stenotic and post-stenotic regions respectively. All the profiles in the daughter artery appear to be different from those of the parent one. The nearly symmetrical shape of the profile at the onset of the stenosis gets perturbed towards the outer wall as the flow advances to the stenotic region and then to post-stenotic region of the branch artery. The considerable effect of constriction on the concentration profile can only be observed in Fig. 8 through a sizeable deviation of the relevant results plotted for $t = 2$s while no such effect is noted on the profile both at the onset and at the offset of the stenosis, represented by the Figs. 7 and 9.

The distribution of the mean concentration of the solute over the entire bifurcated arterial segment for different time periods are presented in Fig. 10. Two peaks are found at two specific locations where the bifurcated artery assumes its maximum constrictions - one at the parent aorta and other at its daughter one while the mean concentration slightly drops down near the apex. These peaks and troughs can be recognized as the disturbing zones of mass

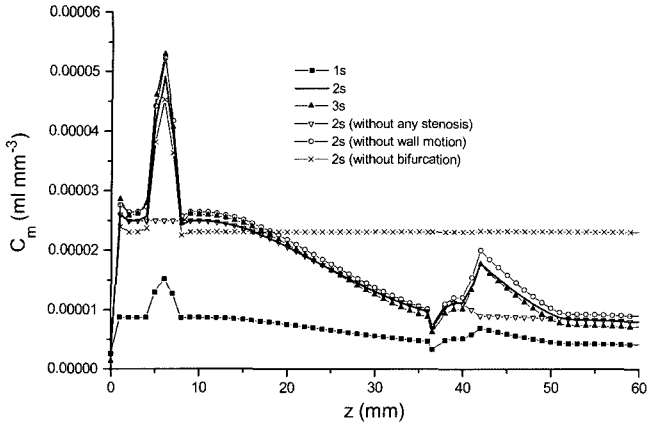

Fig. 10. The distribution of the mean concentration of the solute over the entire bifurcated arterial segment for different time periods.

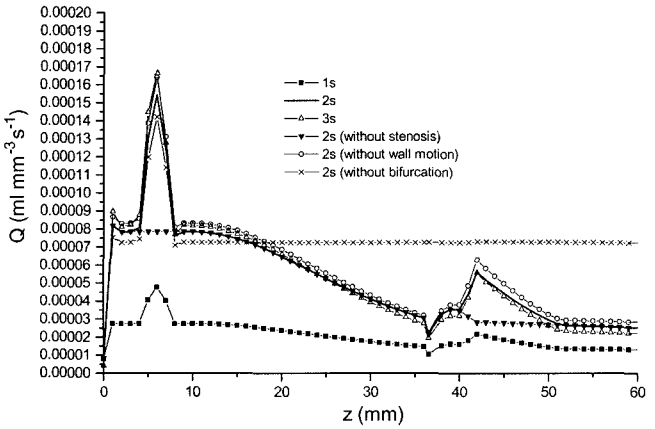

Fig. 11. The net diffusive flux distribution of the solute along the bifurcated arterial tube for different time periods.

transfer through the constricted bifurcated artery. The peaks, however, disappear in the absence of any arterial constrictions and the mean concentration merges completely for the rest of the locations with those for the constricted one. If one withdraws the motion of the wall, the mean concentration appears to increase more at the maximum narrowings of the artery than at other locations. The results corresponding to non-bifurcated artery show uniform distribution of the mean concentration throughout the entire arterial segment excepting only at the constriction site of the parent aorta.

Fig. 11 displays the distribution of the net flux of the solute along the bifurcated arterial tube for different time periods. The diffusive flux increases at the onset of the stenosis in the parent aorta till the constriction assumes maximum followed by a gradual decrease as the constriction assumes minimum and thereafter it decreases to attain the minimum value at the apex and finally increases further towards the other constriction in the daughter artery as well. The results

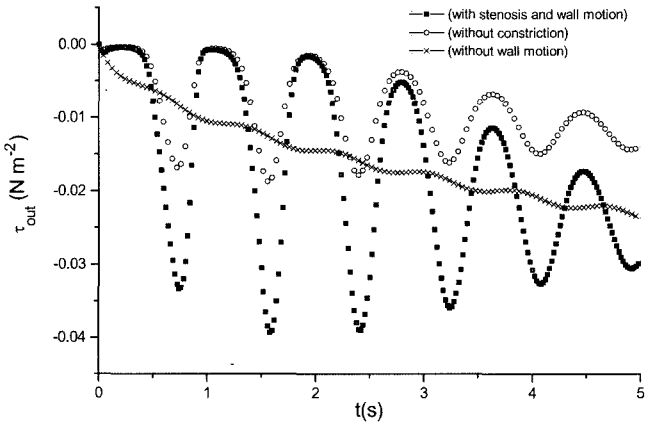

Fig. 12. Behaviour of the wall shear stress on the parent aorta at the constricted region ($z = 6$ mm) with time.

of the present figure represent closely the outline of the distribution of the mean concentration presented in Fig. 10. In consequence there are peaks in the mean concentration at the position of maximum diffusive flux along the bifurcated artery resulting in maximum mass transport in the constricted regions compared to the rest of the locations of the artery.

The variations of the wall shear stress with time in the parent aorta at $z = 6$ mm where the aorta assumes its maximum narrowing are presented in Fig. 12. The corresponding results in the absence of constriction and the absence of wall motion as well are also plotted in the present figure. It appears that the wall shear stress declines from zero at the onset of the cardiac cycle followed by several fluctuations about certain amplitude which finally dissipate towards the large advancement of time. In the absence of stenosis, the stresses experience smaller fluctuations which help estimating the effect of constriction on the shear stresses develop in the parent arterial wall. However, such undulating characteristics completely disappears when the wall motion is withdrawn from the present system. All the stresses mentioned above are compressive in nature as they do appear to be all time negative.

Fig. 13 illustrates the time behaviour of the shear stress on the daughter outer wall at $z = 45$ mm corresponding to the constricted region. Unlike those of the parent aorta, the daughter outer wall experiences stress fluctuations from positive to negative, negative to positive and so on forming several flow separation zones. Such fluctuations eventually dissipate with large passage of time. One may note that the effect of stenosis is meager on the stress values of the daughter outer wall while the effect of wall motion is quite significant. The absence of wall motion keeps the stress almost steady over the entire time range considered here. It has been suggested that the change of shear stress direction or amplitude within a cardiac cycle may be related to atherogenesis (McDonald, 1974). It has also been specu-

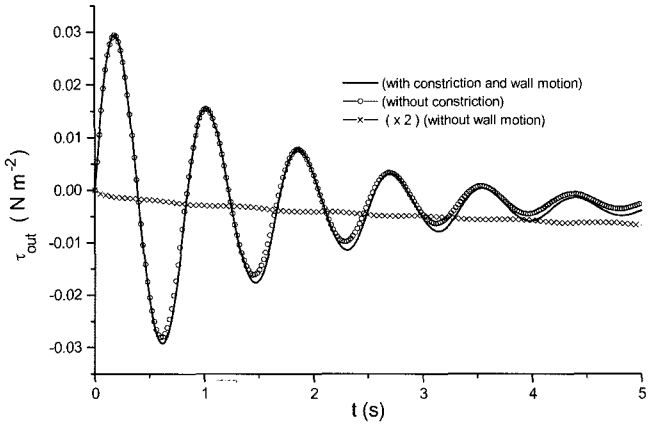

Fig. 13. Time behaviour of the shear stress on the outer daughter wall at the stenotic region ($z = 45$ mm).

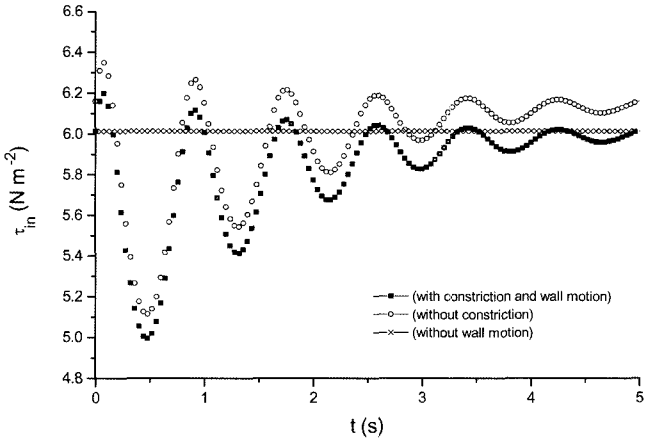

Fig. 14. Time behaviour of the shear stress on the inner daughter wall at the pre-stenotic region ($z = 40$ mm).

lated by Fischer *et al.* (1980) that the increased collagen production resulting from the pulsatile wall stretch due to the pulsatile pressure gradient may be an initiating event in the vessel wall injury leading to atherogenesis. Thus the observations made in the present figure agree well with this hypothesis and it is believed to provide some understanding regarding the formation of atherosclerosis leading to the malfunction of the circulatory system.

The unsteady behaviour of the shear stress on the inner daughter wall at three specific locations corresponding to pre-stenotic ($z = 40$ mm), stenotic ($z = 45$ mm) and post-stenotic ($z = 51$ mm) regions are illustrated in Figs. 14, 15 and 16, respectively. The respective figures also include the corresponding results by disregarding the presence of constriction and the wall distensibility in order to estimate their effects on the inner daughter wall stress phenomena. In the presence of constriction in the arterial lumen and the wall motion, the stress characterizes to be positive with undulating feature all at the pre-stenotic, stenotic and post-stenotic regions in which the stress magnitudes gradually diminish as one proceeds along the daughter artery. The effect of stenosis on the stress characteristics appears to be maximum only in the constricted region while it is moderate in the pre-stenotic region and meagre in the post-stenotic region. The deviation of the effect of constriction as observed from Figs. 14 and 16 shows that the peak stresses at the stenotic region to enhance and troughs to shrink considerably in the absence of constriction while conversely, a meagre changes of the peak stresses to shrink and troughs to enhance at the post-stenotic region is noted for a constriction-free artery. However, the effect of wall distensibility on those stresses appears to have considerable influence on all the chosen locations of the daughter artery.

Fig. 17 exhibits the results for the diffusive flux of the solute at the parent outer wall corresponding to the maximum constricted region at $z = 6$ mm. The shear-dependent

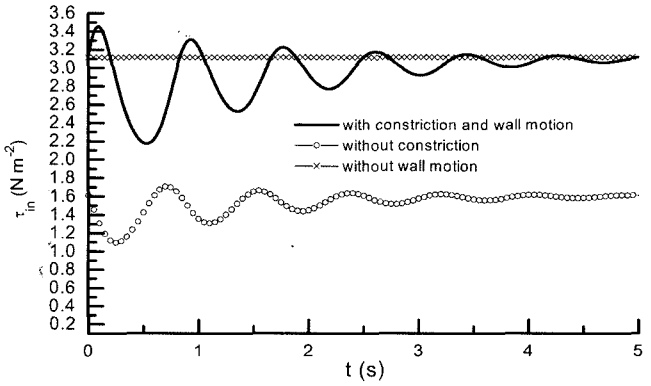

Fig. 15. Time variation of the shear stress on the inner daughter wall at the stenotic region ($z = 45$ mm).

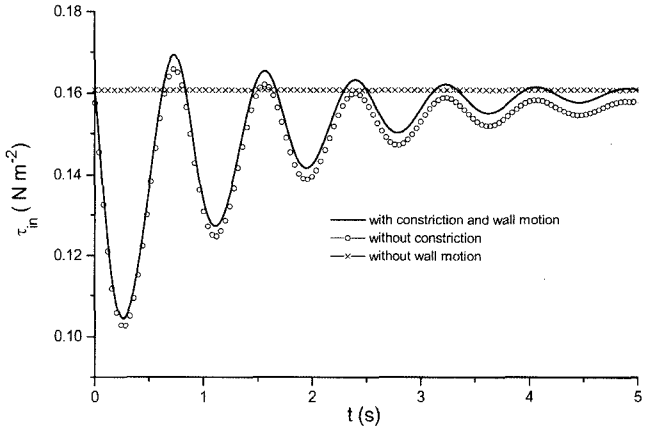

Fig. 16. Time variation of the shear stress on the inner daughter wall at the post-stenotic region ($z = 51$ mm).

wall flux keeps on increasing with pulsatile nature as the time advances while a reverse phenomenon of the wall shear stress is observed as noted in Fig. 12. The magnitudes with the undulating characteristics of the wall flux

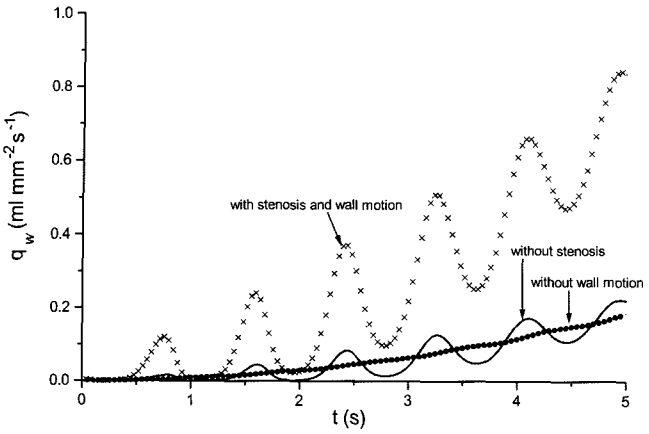

Fig. 17. The diffusive flux of the solute at the outer wall (parent) at the maximum constricted site ($z = 6$ mm) with time.

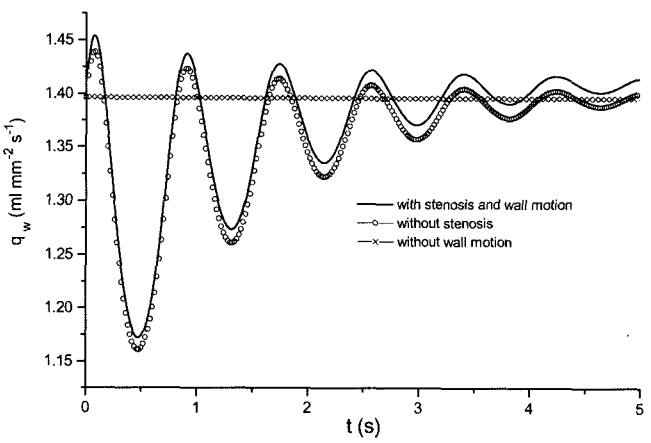

Fig. 19. Unsteady behaviour of the diffusive flux of the solute at the inner wall of the daughter artery in the pre-stenotic region ($z = 40$ mm).

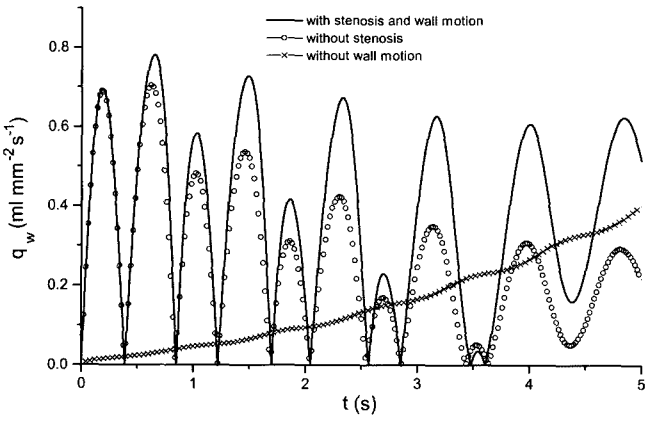

Fig. 18. Unsteady behaviour of the diffusive flux of the solute at the daughter wall corresponding to the constricted region ($z = 45$ mm).

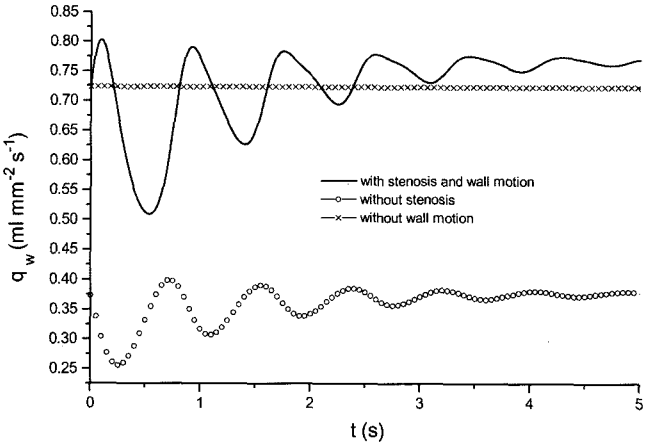

Fig. 20. Unsteady behaviour of the diffusive flux of the solute at the inner wall ofthe daughter artery in the constricted region ($z = 45$ mm).

get considerably reduced in the absence of stenosis and hence the effect of constriction on the diffusive flux of the parent aorta can be measured quantitatively from the deviation of the results obtained. However, no fluctuations appear in the nature of the wall flux when the wall distensibility is totally disregarded. That means, if the vascular wall motion is restricted to rigidity then the wall flux increases almost linearly with time which appears to be quite close to the mean wall flux corresponding to constriction-free diffusive wall flux.

Unlike the behaviour of the wall flux at the parent aorta, the outer daughter wall experiences the diffusive flux with time corresponding to the stenotic region by a sequence of fluctuations as noted in Fig. 18. Here the fluctuations are quite rapid and the peaks are also oscillatory for some time until $t = 3.1$s and then they remain almost steady for rest of the time shown in the present figure. In the absence of constriction, the diffusive wall flux gets reduced considerably when the peaks are lowered to a great extent and hence the presence of stenosis influences the maximum wall flux appreciably. The feature of a gradual increasing trend of the wall flux in the absence of wall motion with the advancement of time does make sense in a way to record the effect of wall distensibility in the present scenario. Although the diffusive wall flux of the solute for a rigid artery increases with time, their magnitudes are quite smaller than those of a flexible artery.

The results of Figs. 19-21 illustrate the unsteady characteristics of the diffusive flux of the solute at the inner wall of the branch artery in three specific locations of $z =$ 40 mm, 45 mm and 51 mm corresponding to the pre-stenotic, stenotic and the post-stenotic regions respectively. The wall flux of the solute drops largely towards the first cardiac cycle followed by the fluctuating trend of increase and decrease which eventually dissipate with large passage of time. Such behaviour is observed in both the onset and

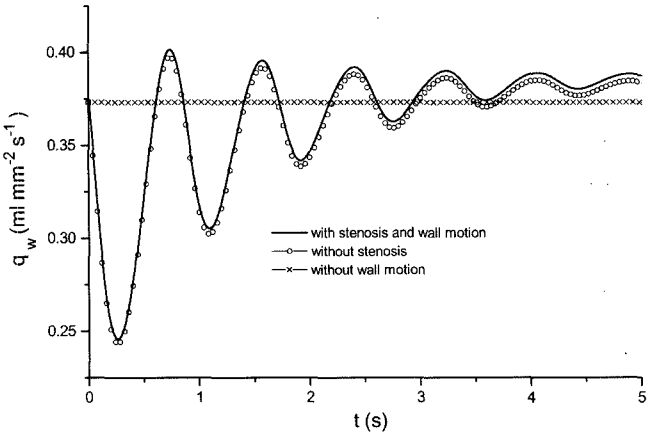

Fig. 21. Unsteady behaviour of the diffusive flux of the solute at the inner wall of the daughter artery in the post-stenotic region ($z = 51$ mm).

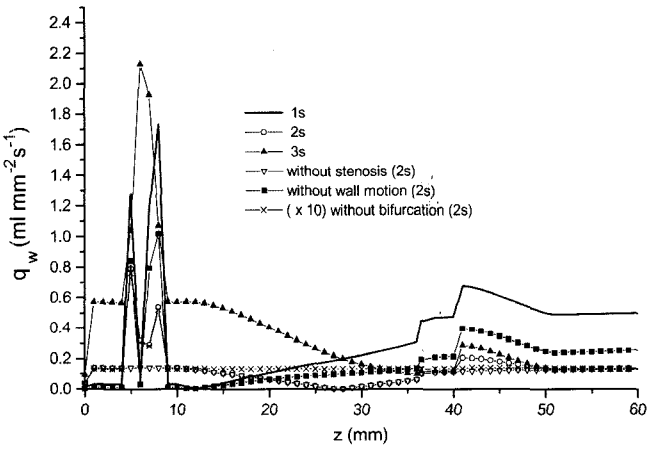

Fig. 22. Distribution of the diffussive flux of the solute at the outer wall of the entire bifurcated arterial segment at different times.

the offset of the constriction with a variance of magnitudes. The wall flux or the flow rate of the solute appears to be higher in magnitude in the pre-stenotic region than that in the post-stenotic region as noted in Figs. 19 and 21. However, in the stenotic region the diffusive wall flux behaves differently forming smaller irregular fluctuations with time which rapidly dissipate. The effect of constriction is recorded more on the wall flux in the stenotic region than in the non-stenotic regions. One may note from the result of the present figures that the peak diffusive wall flux in the constricted zone becomes smaller than that in the pre-stenotic region and larger than the same in the post-stenotic region. The vessel wall rigidity helps the wall flux of the solute free from any fluctuations other than magnitudes irrespective of the choice of these critical locations of the daughter artery.

Finally, the concluding Fig. 22 of the present paper shows the distribution of the mass transfer of the solute at the outer wall of the entire bifurcated arterial segment at different times. The wall flux appears to have its maximum at the specific locations of maximum constrictions for all time where the mean concentration of oxygen is high. One may note that a high wall flux means that the concentration gradient is high which results in a low concentration at the wall compared with the flowing blood if the direction of the flux is outwards as in the present case. The present results agree qualitatively well with Back *et al.* (1977) who found a peak in wall flux just upstream the location of maximum constriction. Here too, the influences of arterial constriction, the vassal wall distensibility and of the arterial bifurcation on the diffusive flux distribution at the arterial wall are quantified in order to indicate their importance in the roles played for the development of atherosclerotic lesions. The potentiality of treating simultaneously the blood phase transport and shear-dependent variations in intimal permeability of the present theoretical model is certainly believed to be a considerable feature for a physiologically realistic bifurcated flow model of mass transfer processes.

7. Concluding Remarks

The unsteady flow of blood and convective diffusion processes was studied through a two-dimensional constricted bifurcated arterial model. Although a two-dimensional model bifurcation can not provide three-dimensional information, but fortunately major atherogenic regions around arterial bifurcations are more concentrated in bifurcation planes coinciding with two-dimensional planes especially in early stages of atherogenesis (Kashihara *et al.*, 1988). Since the arteries forming bifurcations are symmetrical about the trunk axis, there is no loss of generality on the assumption of axisymmetric flow phenomena and hence this assumption does not break down when the recirculation zone is comparable to size to the diameter of daughter branch. This assumption of axial symmetry has been validated substantially through the exhibition of the behaviour of the axial velocity profile in the branch artery [cf. Fig. 2(c)]. The relevant parameters describe the physiological situations for the transport of oxygen in the bifurcated arteries. The finite difference technique through an explicit iterative scheme has been employed to obtain numerical results with desired accuracy. The potentiality of treating simultaneously the blood media transport and shear dependent variations in intimal permeability of the present model seems to be an important characteristic for a physiologically realistic simulation of bifurcated flow and mass transfer processes. The salient observations of the present unsteady model study may be listed as follows:

- The concentration of the solute increases with the arte-

rial narrowing and with bifurcation but decreses with wall distensibility.

- The effects of stenosis and the wall distensibility on the concentration profile are megre at the apex compared to the other locations of the parent duct.
- The concentration profile in the daughter arteries are different from those of the parent one.
- The diffusive flux of the solute increases with the arterial narrowing and it becomes minimum at the apex.
- The peaks in the mean concentration corresponding to maximum diffusive flux result in maximum mass transport in the constricted regions only.
- The influence of stenosis is meager on the stress values of the outer daughter wall while the effects of wall distensibility is significant.
- The diffusive wall flux increases in the absence of wall motion which appears to be closure to the mean wall flux corresponding to constriction-free diffusive wall flux.
- The peak diffusive wall flux in the constricted zone becomes smaller than that in the pre-stenotic region and larger than the same in the post-stenotic region.

Acknowledgements

Authors are highly grateful to the reviewers for their valuable comments and suggestions. The present work is part of the Special Assistance Programme [Grant No. F.510/8/DRS/ 2004(SAP-I)] sponsored by the University Grants Commission (UGC), New Delhi, India.

References

Back, L.H., J.R. Radbill and D.W. Crawford, 1977, Analysis of oxygen transport from pulsatile, viscous blood flow in diseased coronary arteries of man, *J. Biomech.* **10**, 763-774.

Bassingthwaitghte, J.B., A. Deussen, D. Beyer, I.S. Chan, G.R. Raymond, R.B. King, T.R. Bukowski, J.D. Ploger, K. Kroll, J. Revenaugh, J.M. Link and K.A. Krohn, 1992, Oxygen transport in the myocardium, *Adv. Biological Heat and Mass Transfer ASME* **231**, 113-119.

Burton, A.C., 1996, Physiology and Biophysics of the Circulation: Introductory Text, Year Book Medical Publisher, Chicago.

Chakravarty, S. and P.K. Mandal, 1997, An analysis of pulsatile flow in a model aortic bifurcation, *Int. J. Engng. Sci.* **35**, 409-422.

Deshpande, M., D. Giddens and R. Mabon, 1976, Steady flow through modelled vascular stenoses, *J. Biomech.* **9**, 165-174.

Fischer, G.M., M.L. Swain and K. Cherian, 1980, Pulsatile distension and vascular collagen synthesis in the rabbit, *Blood Vessels* **17**, 215.

Fridman, M.H. and L.W. Ehrlich, 1975, Effect of spatial variations in shear on diffusion at the wall of an arterial branch, *Cric. Res.* **37**, 446-454.

Fry, D.L., 1968, Acute vascular endothelial changes associated with increased blood velocity gradients, *Cric. Res.* **22**, 165-197.

Imaeda, K. and F.O. Goodman, 1980, Analysis of nonlinear pulsatile blood flow in arteries, *J. Biomech.* **13**, 1007-1022.

Jo, M., R.O. Dull, T.M. Hollis and J.M. Tarbell, 1991, Endothelial albumin permeability is shear dependent, time dependent and reversible, *Am. J. Physiol.* **260**, H1992.

Kashihara, M., K. Matsumoto and J. Cervos-Navarro, 1988, Observations on carotid bifurcation, atherosclerosis in human cadavers, In: Role of Blood Flow in Atherogenesis (Edited by Yoshide, Y., Yamaguel, T., Caro, C.G. and Nevem, R.M.) *Proc. Int. Symp.* **19**, Springer-Verleg, Tokyo.

Liepsch, D.W. 1990, Effect of blood flow parameters on flow patterns in arterial bifurcations: studies in models, in Blood Flow in Large Arteries: Applications to Atherogenesis and Clinical Medicine, D.W. Liepsch, Ed., S. Karger, Basel, 63.

Liepsch, D.W. and S.T. Moravec, 1984, Pulsatile flow of non-Newtonian fluid in distensible models of human arteries, *Biorheology* **21**, 571-586.

Ling, S.C. and H.B. Atabek, 1972, A nonlinear analysis of pulsatile blood flow in arteries, *J. Fluid Mech.* **55**, 492-511.

Lou, Z. and W.J. Yang, 1992, Biofluid dynamics at arterial bifurcations, *Crit. Rev. Biomed. Engng.* **19**, 455-493.

Ma, P., X. Li and D.N. Ku, 1994, Heat and mass transfer in a separated flow region for high Prandtl and Schmidt numbers under pulsatile conditions, *Int. J. Heat Mass Transfer* **37**, 2723-2736.

McDonald, D.A., 1974, Blood Flow in Arteries, 2nd ed. Edward Arnold, London.

McIntire, L.V. and R. Tran-Son Tay, 1989, Concentration of materials released from mural platelet aggregates: flow effects, in Biomedical Engineering, Eds., W.J. Yang and J.L. Chun, Hemisphere, New York, 229-245.

Milnor, W.R., 1982, Haemodynamics, Williams and Williams, Baltimore.

Pedley, T.J., 1980, The Fluid Mechanics of Large Blood Vessels, Cambridge University Press, Cambridge.

Reidy, M.A. and D.E. Bowyer, 1997, Scanning electron microscopy of arteries: the morphology of aortic endothelium in hemodynamically stressed areas associated with branches, *Atherosclerosis* **26**, 181.

Rappitsch, G. and K. Perktold, 1996, Computer simulation of convective diffusion processes in large arteries, *J. Biomech.* **39**, 207-215.

Singh, M.P., R.K. Sharan, R.K. Saxena and I. Malhotra, 1982, A theoretical model for the exchange of gases in the systemic capillaries and the surrounding tissues under compression an application in underwater physiology, in Finite Element Flow Analysis, Ed. T. Kawai, University of Tokyo Press, North Holland, Amsterdam, 867-875.

Tarbell, J.M., 1993, Bioengineering studies of the endothelial transport barrier, *BMES Bulletin* **17**, 35-39.

Womersley, J.R., 1957, An elastic tube theory of pulse transmission and oscillatory flow in mammalian arteries, Wright Air Development Centre Technical Report TR 56-6114.

Appendix

The discretised expressions of the coefficients $A^k_{i,j}$, $B^k_{i,j}$, $C^k_{i,j}$ etc. of (28) should be read as

$$A^k_{i,j} = \xi_j \frac{\partial R^k_i}{\partial t} + \frac{\partial R^k_{2i}}{\partial t} + \frac{\mu}{\rho(\xi_j R^k_i + R^k_{2i})},$$

$$B^k_{i,j} = -\frac{\mu}{\rho}\left[\frac{\partial^2 R^k_{2i}}{\partial z^2} + \xi_j \frac{\partial^2 R^k_i}{\partial z^2} - \frac{2}{R^k_i}\frac{\partial R^k_i}{\partial z}\left(\xi_j \frac{\partial R^k_i}{\partial z} + \frac{\partial R^k_{2i}}{\partial z}\right)\right],$$

$$C^k_{i,j} = \left(\frac{-R^k_{2i}}{\xi_j R^k_i + R^k_{2i}}\right) u^k_{i,1},$$

$$D^k_{i,j} = -\frac{R^k_{1i}\xi_j^2}{\xi_j R^k_i + R^k_{2i}}\left(\alpha \frac{\partial R^k_{1i}}{\partial t} - \frac{R^k_{2i}}{R^k_{1i}} u^k_{i,j}\right)(2-\xi_j^2),$$

$$F^k_{i,j} = \frac{\mu}{\rho (R^k_i)^2 (\Delta\xi)^2}\left[1 + \left(\xi_j \frac{\partial R^k_i}{\partial z} + \frac{\partial R^k_{2i}}{\partial z}\right)^2\right],$$

$$G = \frac{\mu}{\rho(\Delta z)^2}, \quad H = -\frac{1}{2\Delta z}$$

while those of d^k_{ij}, e^k_{ij}, f^k_{ij} etc. involved in (29) are of the form given by

$$d^k_{ij} = a^k_{ij} + b^k_{ij}, \quad e^k_{ij} = b^k_{ij} - a^k_{ij}, \quad f^k_{ij} = \frac{w^k_{i,j}}{2\Delta z} + \frac{D}{(\Delta z)^2},$$

$$g^k_{ij} = \frac{D}{(\Delta z)^2} - \frac{w^k_{i,j}}{2\Delta z} \quad \text{and} \quad l^k_{ij} = -2\left(b^k_{ij} + \frac{D}{(\Delta z)^2}\right)$$

in which

$$a^k_{ij} = \frac{1}{2R^k_i \Delta\xi}\left[\left(\xi_j \frac{\partial R^k_i}{\partial t} + \frac{\partial R^k_{2i}}{\partial t}\right) + \left(w^k_{i,j} + \frac{D}{R^k_i}\frac{\partial R^k_i}{\partial z}\right)\left(\xi_j \frac{\partial R^k_i}{\partial z} + \frac{\partial R^k_{2i}}{\partial z}\right) - u^k_{i,1}\right.$$
$$\left. -D\left(\xi_j \frac{\partial^2 R^k_i}{\partial z^2} + \frac{\partial^2 R^k_{2i}}{\partial z^2}\right) + \frac{D}{\xi R^k_i + R^k_{2i}}\right]$$

and

$$b^k_{ij} = \frac{D}{(R^k_i \Delta\xi)^2}\left[1 + \left(\xi_j \frac{\partial R^k_i}{\partial z} + \frac{\partial R^k_{2i}}{\partial z}\right)^2\right].$$